Supporting information:

Single-Molecule Electrochemical Imaging Resolves the Midpoint Potentials of Individual Fluorophores on Nanoporous Antimony-Doped Tin Oxide

Jin Lu[ab‡*], Matthew D. Lew[ab*]

[a] *Preston M. Green Department of Electrical and Systems Engineering, McKelvey School of Engineering, Washington University in St. Louis, MO, 63130, USA*

[b] *Institute of Materials Science and Engineering, Washington University in St. Louis, MO, 63130, USA*

[‡] *Current position: CAS Key Laboratory for Biomedical Effects of Nanomaterials and Nanosafety, National Center for Nanoscience and Technology, Beijing, 100190, China*

[*] *Co-corresponding authors. E-mail address: luj@nanoctr.cn, mdlew@wustl.edu*

Table of Contents

List of Figures

Supplementary Figures

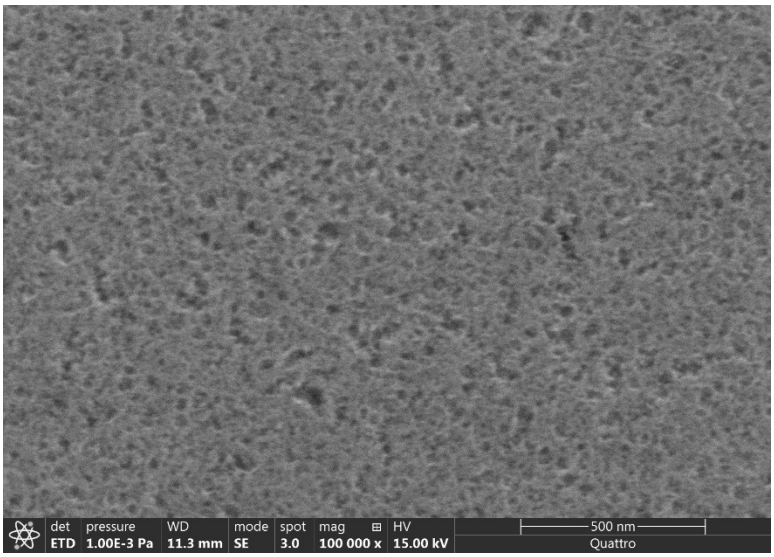

Figure S1 | Scanning electron microscope (SEM) image of a nanoporous antimony-doped tin oxide (nATO) film on an indium tin oxide (ITO) coverslip. Scale bar: 500 nm. The image was captured on Thermofisher Quattro S Environmental SEM.

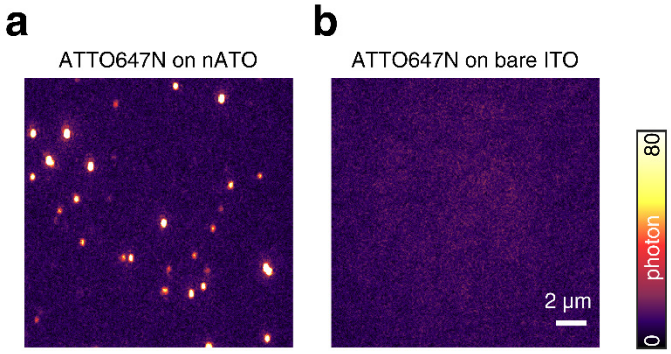

Figure S2 | Single-molecule fluorescence images of ATTO647N on (a) an nATO electrode and (b) a bare ITO electrode (exposure time: 100 ms). Scale bar: 2 µm.

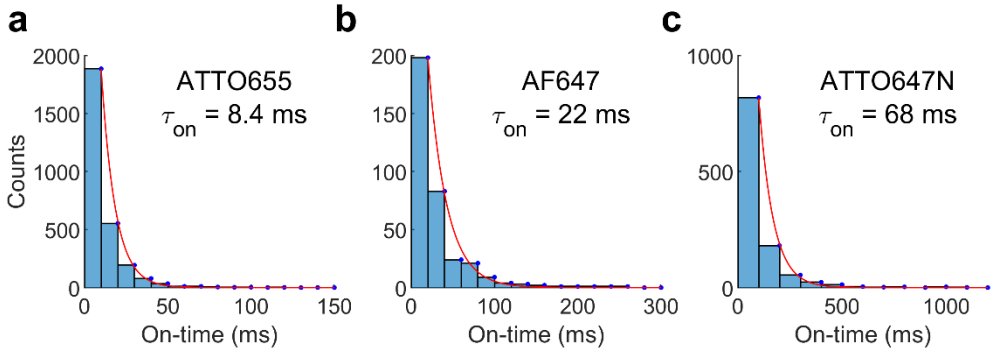

Figure S3 | Single-molecule fluorescence burst durations (on-times) of (a) ATTO655, (b) AF647, and (c) ATTO647N. Red solid lines indicate fits to an exponential decay, yielding the reported average on-times τ_{on}.

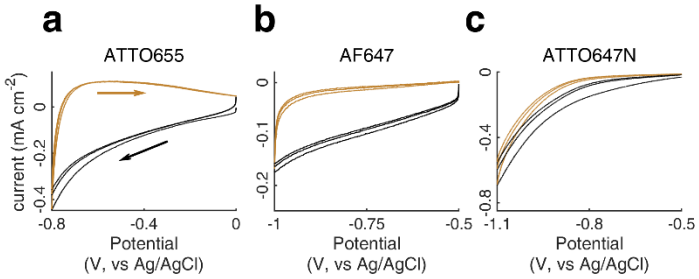

Figure S4 | Cyclic voltammetry of (a) ATTO655, (b) AF647, and (c) ATTO647N in 1 M $NaNO_3$. The plots correspond to the SMEC imaging in Figure 1. Black and dark yellow trajectories represent the forward and reverse scans, respectively.

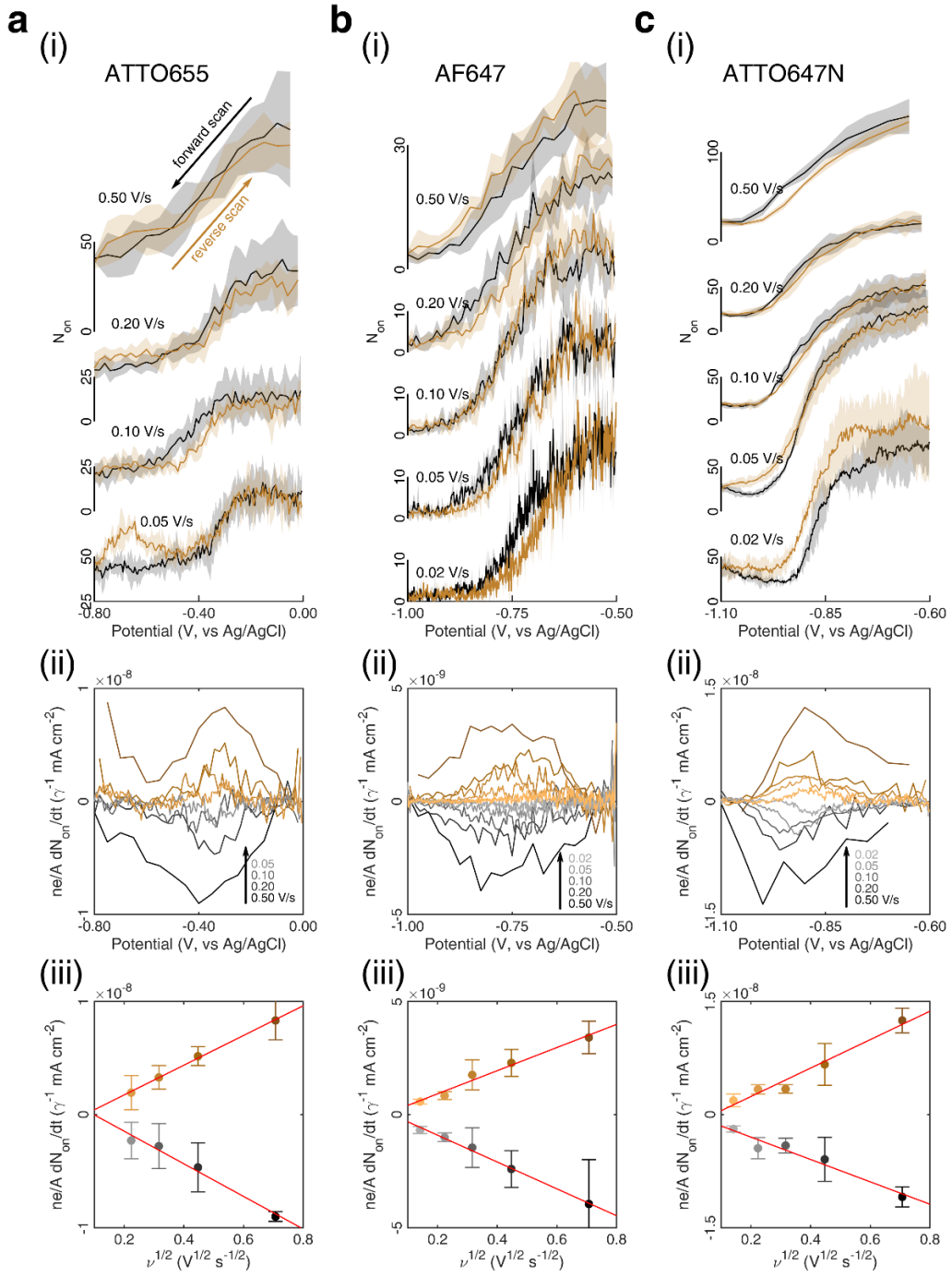

Figure S5 | (i) Number N_{on} of fluorescent molecules over time observed during SMEC imaging of potential scans and (ii) its time derivative for (a) ATTO655, (b) AF647, and (c) ATTO647N at different scan rates. (iii) The square root of scan rate dependence of the peak values within the time derivative traces in (ii). Red lines are linear fits, n is the number of electrons transferred in a redox process, e is elementary charge, and A is electrode surface area.

Discussion of Figure S5

The prepared nATO coating enables us to capture SM fluorescence images and monitor electrochemical responses of single dye molecules. As reported previously,[1] the decreased number of detected single dye molecules ($\Delta \mathrm{N_{on}}$) at certain applied potentials is proportional to the total number of dye molecules that have been reduced ($\gamma \Delta \mathrm{N_{on}}$), and thus the total charge passed through the electrode is given by

$$Q = n\gamma e \Delta \mathrm{N_{on}},$$

where e is elementary charge. Therefore, the time derivative of the detected number ($\mathrm{d}\mathrm{N_{on}}/\mathrm{d}t$) measures the faradaic current,

$$i = \mathrm{d}Q/\mathrm{d}t = n\gamma e \left(\frac{\mathrm{d}\Delta \mathrm{N_{on}}}{\mathrm{d}t}\right).$$

For all three tested probes, their peak values of $\mathrm{d}\mathrm{N_{on}}/\mathrm{d}t$ at various scan rates are all proportional to the square root of the scan rate (Fig. S5a-c(iii)).

These data follow the Randles–Sevcik equation[2] for an electrochemically reversible electron transfer process with a freely diffusing redox species. The peak current is thus expressed as

$$i_{\mathrm{p}} = 0.446nFAC^0 \left(\frac{nF\nu D_{\mathrm{o}}}{RT}\right)^{1/2},$$

where R is the gas constant, T is the absolute temperature, F is Faraday's constant, ν is the scan rate, n is the number of electrons transferred in the redox reaction, A is the electrode surface area, C^0 is the bulk concentration of the analyte, and D_{o} is the diffusion coefficient of the analyte. Thus, we conclude that all observed direct electrochemical reductions on nATO follow diffusion-controlled electrochemical kinetics.

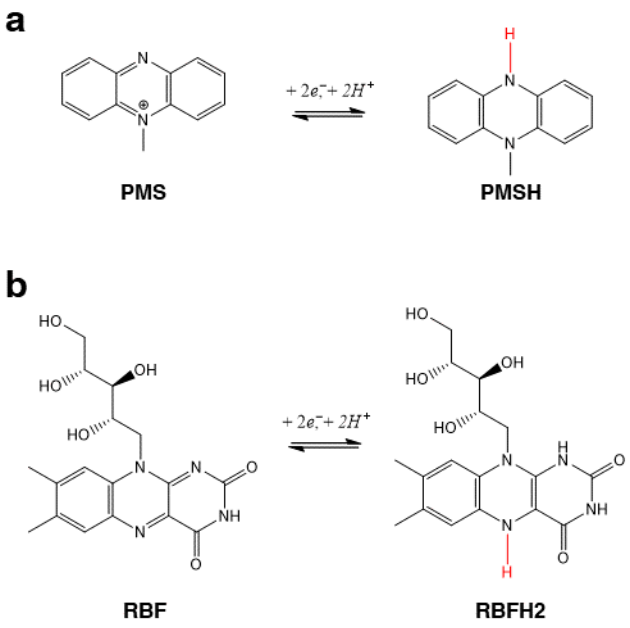

Figure S6 | Chemical structures and electrochemical reduction reactions of (a) PMS[3] and (b) riboflavin (RBF)[4].

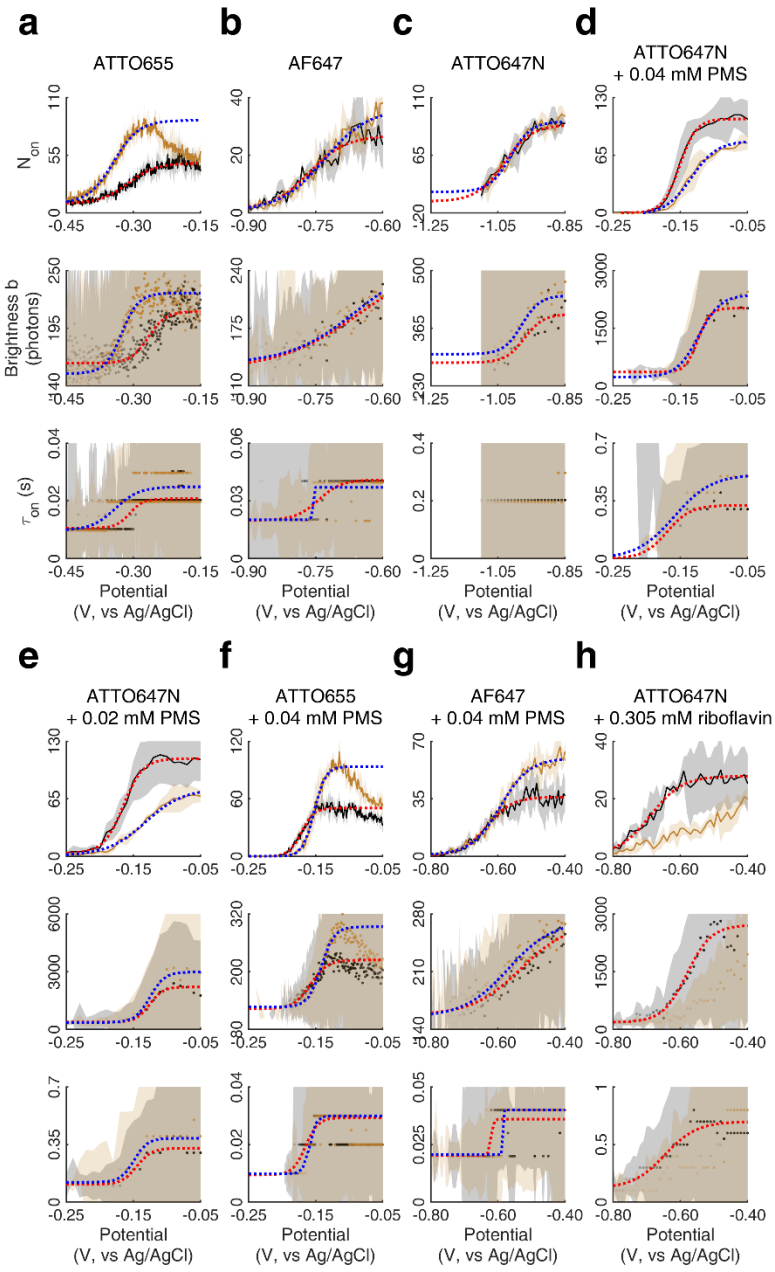

Figure S7 | Sigmoid curve fitting of single-molecule number (N_{on}), brightness (b), and burst duration (τ_{on}) trajectories shown in Figures 1 and 2 in the main text. (a) ATTO655, (b) AF647, and (c) ATTO647N profiles in Figure 1. (d) ATTO647N+0.04 mM PMS, (e) ATTO647N+0.02 mM PMS, (f) ATTO655+0.04 mM PMS, (g) AF647+0.04 mM PMS, and (h) ATTO647N+0.305 mM riboflavin trajectories in Figure 2. Here, we fit a potential range centered at the on-off transition of the fluorescent molecules, rather than the entire range of applied potential. Red dotted line: fitting to the forward scan (black); blue dotted line: fitting to the reverse scan (dark yellow). There are no successful fits of τ_{on} of ATTO647 in (c). Fitting is not carried out on the reverse scans of ATTO647N+riboflavin in (h).

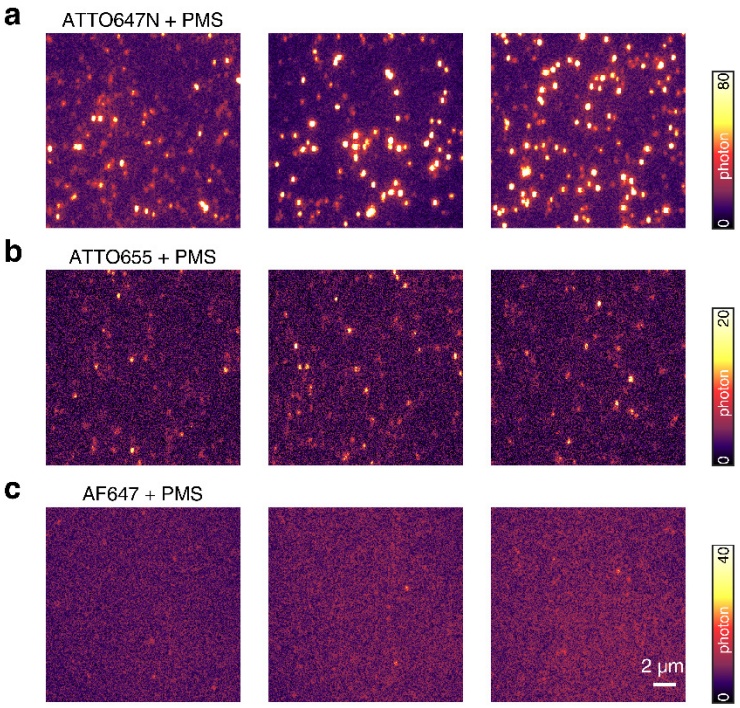

Figure S8 | Representative raw images of (a) ATTO647N+0.04 mM PMS, (b) ATTO655+0.04 mM PMS, and (c) AF647+0.04 mM PMS within the initial 200 mV of forward scans. Scale bar: 2 μm.

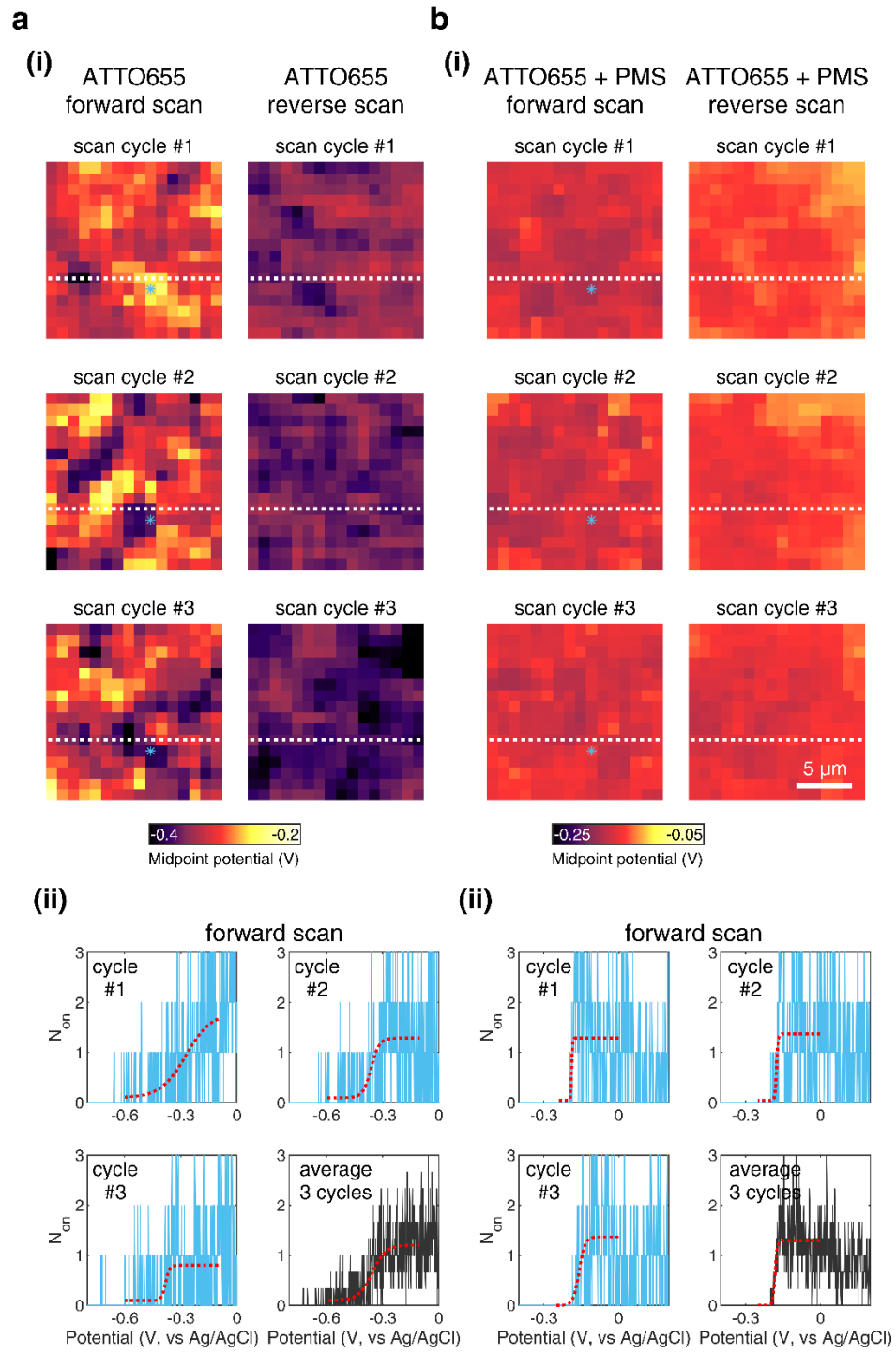

Figure S9 | (i) Midpoint potential maps calculated from each forward and reverse scan cycle of ATTO655 (a) without and (b) with 0.04 mM PMS. Scale bar: 5 μm. The white dotted lines indicate the line profiles drawn in Figure 3a,b. (ii) The raw N_{on} responses of one representative 1×1 μm^2 bin (indicated by blue asterisks in (i)) from each forward scan cycle (blue solid line) and the averaged response (black solid line). The red dotted profiles represent the fitting to a sigmoid function.

Discussion of Figure S9

We defined a 3 μm × 3 μm sliding window and move it along the x and y directions in 1 μm increments over the entire raw image (17.55 μm × 17.55 μm). At each window position, for each forward or reverse scan cycle, trajectories of the number of detected molecules (N_{on}) with respect to applied potential was collected and fit to a sigmoid function (Eqn. 2 in the main text) (cycle #1-#3, blue profiles in Figs. S9a(ii) and S9b(ii)). The fitting results (midpoint potential) were used to generate the midpoint potential maps for each scan (Figs. S9a(i) and S9b(i)) with a bin size of 1 μm.

In the case of ATTO655 dye without PMS, for the same bin location (highlighted by blue asterisks in Fig. S9a(i), for example), we observed strongly varying midpoint potentials between the cycles. This variation is most likely due to the low number of dye molecules that stochastically reside within the sliding window. Moreover, the electron transfer rate between the single dye molecule and the nATO electrode also varies. These effects cause the inconsistent N_{on} response patterns and thus the distinct fitting results between cycles.

In contrast, in the presence of PMS that promotes higher rates k_{f2} as discussed in main text. As a result, the midpoint potential maps look more consistent between cycles (Fig. S9b), despite having similar N_{on}-event density compared to the non-PMS case.

Alternatively, to characterize the spatial heterogeneity of electron-transfer rates on nATO, rather than resolving single-molecule electron transfer events, we first calculated the average N_{on} response from all three scan cycles, fit it to a sigmoid function (average 3 cycles, black profiles in Figs. S9a(ii) and S9b(ii)), and generated averaged midpoint potential maps (Fig. 3a, b). These maps (Fig. 3a, b) eliminate the stochastic behavior of single molecules, and provide more information on the spatial heterogeneity of electron-transfer rates on electrode surface, as discussed in the main text.

Supplementary Note

Eqn. 5 in the main text

$$E_{\mathrm{D},2} = E^{\mathrm{o}}_{\mathrm{PMS/PMSH}} - 0.409\frac{RT}{F} + \frac{RT}{2F}\ln\left(\frac{RTk_{\mathrm{f2}}}{F\nu}\frac{[\mathrm{PMS}]^2}{[\mathrm{dye}]}\right) \quad \text{(Eqn. 5)}$$

is adapted from equation 2.21 in the book of *Elements of Molecular and Biomolecular Electrochemistry (2019 edition)* [5].

As discussed in the main text, total catalysis is reached when there is a large homogeneous rate constant and a low dye molecule concentration.

In this case, for the reaction of

$$\mathrm{P} + \mathrm{ne}^- \leftrightarrow \mathrm{Q} \quad \text{(Rxn. S1)}$$

$$\mathrm{Q} + \mathrm{A} \underset{\leftarrow}{\overset{\mathrm{k_e}}{\rightarrow}} \mathrm{P} + \mathrm{B}\,, \quad \text{(Rxn. S2)}$$

the dimensionless expression of potential (ξ^{tc}) is expressed as

$$\xi^{\mathrm{tc}} = -\frac{F}{RT}\left(E - E^0_{\mathrm{P/Q}}\right) + \frac{1}{2}\ln\left(\frac{RT}{F\nu}\frac{k_{\mathrm{e}}{C^0_{\mathrm{P}}}^2}{C^0_{\mathrm{A}}}\frac{D_{\mathrm{P}}}{D_{\mathrm{A}}}\right), \quad \text{(Eqn. S1)}$$

and its peak position is

$$\xi^{\mathrm{tc}}_p = 0.409\,. \quad \text{(Eqn. S2)}$$

Rxn. S1, S2 are from Section 2.2.6, and Eqn. S1, S2 are directly from Section 7.2.7.1 of *Elements of Molecular and Biomolecular Electrochemistry (2019 edition)*[5], respectively.

Therefore, by combining Eqn. S1 and Eqn. S2, the peak potential is expressed as

$$E_{\mathrm{p}} = E^0_{\mathrm{P/Q}} - 0.409\frac{RT}{F} + \frac{RT}{2F}\ln\left(\frac{RT}{F\nu}\frac{k_{\mathrm{e}}{C^0_{\mathrm{P}}}^2}{C^0_{\mathrm{A}}}\frac{D_{\mathrm{P}}}{D_{\mathrm{A}}}\right). \quad \text{(Eqn. S3)}$$

We assume the diffusion coefficients (D) of all species in reactions (1), (2), (Rxn. S1), and (Rxn. S2) are identical. We also let the potentials $E_{\mathrm{p}} = E_{\mathrm{D},2}$ and $E^0_{\mathrm{P/Q}} = E^{\mathrm{o}}_{\mathrm{PMS/PMSH}}$, the homogeneous rate constant $k_{\mathrm{e}} = k_{\mathrm{f2}}$, and the concentration $C^0_{\mathrm{P}} = [\mathrm{PMS}]$ and $C^0_{\mathrm{A}} = [\mathrm{dye}]$. We therefore obtain Eqn. 5 from Eqn. S3.

Supplementary Movies

Movie S1. SMEC imaging of ATTO655 dye molecules captured during an electrochemical potential sweep between 0 V and –0.8 V at a scan rate of 0.1 V/s in 1 M $NaNO_3$ solution. Scale bar: 5 μm.

Movie S2. SMEC imaging of AF647 dye molecules captured during an electrochemical potential sweep between –0.5 V and –1.0 V at a scan rate of 0.1 V/s in 1 M $NaNO_3$ solution. Scale bar: 5 μm.

Movie S3. SMEC imaging of ATTO647N dye molecules captured during an electrochemical potential sweep between –0.5 V and –1.1 V at a scan rate of 0.1 V/s in 1 M $NaNO_3$ solution. Scale bar: 5 μm.

References

1 J. Lu, Y. Fan, M. D. Howard, J. C. Vaughan and B. Zhang, *J. Am. Chem. Soc.*, 2017, **139**, 2964–2971.

2 N. Elgrishi, K. J. Rountree, B. D. McCarthy, E. S. Rountree, T. T. Eisenhart and J. L. Dempsey, *J. Chem. Educ.*, 2018, **95**, 197–206.

3 O. S. Ksenzhek, S. A. Petrova and M. V. Kolodyazhny, *Bioelectrochemistry Bioenerg.*, 1977, **4**, 346–357.

4 Z. Shi, J. M. Zachara, L. Shi, Z. Wang, D. A. Moore, D. W. Kennedy and J. K. Fredrickson, *Environ. Sci. Technol.*, 2012, **46**, 11644–11652.

5 J. Savéant and C. Costentin, *Elements of Molecular and Biomolecular Electrochemistry*, Wiley, 2019, 113-117.